Measurement 253 (2025) 117762

Contents lists available at ScienceDirect

Measurement

journal homepage: www.elsevier.com/locate/measurement

Guided waves in plates with complex thickness variations: comparison of statistical modeling approaches

Beata Zima [a,*], Jochen Moll [b,c]

[a] Faculty of Mechanical Engineering and Ship Technology, Gdańsk University of Technology, 80-233 Gdańsk, Poland
[b] Department of Physics, Goethe University Frankfurt 60438 Frankfurt, Germany
[c] Department of Mechanical Engineering, University of Siegen 57076 Siegen, Germany

ARTICLE INFO

Keywords:
Guided waves
Irregular plate
Numerical simulations
Random fields
Experimental tests
Innovative systems

ABSTRACT

Guided wave-based techniques are particularly effective for corrosion assessment due to their sensitivity to geometric variations and ability to propagate over long distances. However, most existing approaches rely on simplifying assumptions about thickness distribution, which can introduce inaccuracies in real-world applications, e.g., the thickness reduction due to the corrosion degradation. This study investigates the impact of thickness variability on guided wave propagation in plate-like structures with non-uniform geometry, specifically sinusoidal thickness variations. A combined experimental, numerical, and theoretical approach is employed to analyze wave velocity changes under different statistical assumptions about thickness distribution. The study compares constant-thickness approximations, normal distribution models, and a novel application of Chebyshev's theorem, which provides a more generalized representation of thickness variability. Experimental validation is performed using CNC-fabricated plates with controlled thickness variations, and numerical simulations are conducted using finite element modeling. The results demonstrate that standard assumptions, particularly normal distribution approximations, can introduce significant errors in velocity estimation, whereas the Chebyshev-based approach offers a more accurate and flexible method for modeling non-uniform thickness distributions. These findings provide valuable insights into the development of improved guided wave-based methodologies for corrosion assessment and structural health monitoring.

1. Introduction

In recent decades, non-destructive diagnostic methods based on the propagation of guided waves have garnered significant attention from both researchers and industry professionals [1,2]. A key advantage of these methods is their capability to detect damage that is invisible to the naked eye and cannot be identified through standard visual inspections [3]. Additionally, ultrasonic waves are sensitive to even minor defects, such as cuts or cracks, which enables the early detection of developing damage [4–6]. It is, therefore, unsurprising that non-destructive methods have become highly valued in scientific research, as their proficient application can extend the operational lifespan of structures and reduce maintenance and inspection costs.

Guided waves propagate as dispersive waves, meaning their propagation speed depends on the frequency and the medium's material and geometric properties. Therefore, they are used not only for defect detection and localization but also for characterizing the medium, particularly when its properties are unknown. Since wave velocity is influenced by the material properties of the medium, wave-based methods have been widely employed for the non-destructive evaluation of these parameters [7,8]. This is especially crucial for materials that degrade over time.

Another property frequently utilized in structural diagnostics is the relationship between guided wave velocity and geometric parameters. The velocity of Lamb waves propagating in plates depends on plate thickness [9,10], while waves excited in rods with circular cross-sections are influenced by the rod's diameter [11,12]. This relationship is widely used in applications to assess thickness or diameter, particularly in cases involving corrosion-induced degradation, where these parameters are reduced over time [13–15].

The influence of plate thickness variations as well as the material [16] on wave propagation has been extensively studied in the literature. This includes plates with abrupt, stepwise thickness changes [17–19], plates with linearly varying thickness [20–22], and cases where the

* Corresponding author.
E-mail address: beata.zima@pg.edu.pl (B. Zima).

https://doi.org/10.1016/j.measurement.2025.117762
Received 12 February 2025; Received in revised form 22 April 2025; Accepted 3 May 2025
Available online 4 May 2025

geometry is described by more complex functions [23,24]. It was demonstrated that the thickness changes can be associated with wave reflection [18], triggering of additional wave modes [19,21] propagation of adiabatic modes [20] and wavenumber variations [22]. Recent studies have addressed dispersion and attenuation of Lamb [25] and SH waves in multilayered piezoelectric semiconductor plates with imperfect interfaces [26], as well as the propagation on piezoelectric substrates with periodic surface features such as slight ridges or thin metal strips [27]. These contributions highlight the versatility of analytical and numerical approaches in characterizing guided wave behavior across a wide range of structural configurations and material systems.

Special attention was given to the possibility of solving the inverse problem, i.e., determining the plate thickness based on guided wave measurements. Unfortunately, despite extensive research on wave propagation in plates with variable thickness, certain assumptions are still commonly made. On one hand, these assumptions simplify the problem's solution; on the other hand, they may limit the applicability of the developed methods or lead to significant errors. One common assumption is that a plate or another structure with variable thickness—such as one subjected to corrosion-induced degradation—can be approximated as a plate with a constant thickness. This approach is then used to estimate material loss due to corrosion [15]. Adopting this assumption significantly simplifies the analysis, as only a single unknown variable needs to be determined. However, this assumption prevents the identification of extreme thickness values, particularly the minimum thickness, which tends to be overestimated in this approach. This is critical from a structural integrity standpoint, as the minimum thickness plays a key role in assessing the strength, and hence safety, of the construction.

Another simplifying assumption is that thickness variations occur in discrete steps, allowing the entire plate geometry to be characterized by a few parameters (i.e., several discrete thickness values) [18,28]. This assumption enables the grouping of different thickness values into a few distinct sets. It proves highly effective when a sudden thickness change is expected (e.g., due to the detachment of a layer). However, in cases where thickness variations are more gradual, this approach often only provides an approximation of the actual geometry, which may not be fully accurate in many real-world scenarios.

Simplified assumptions are often applied even to plates with highly complex geometries, such as corroded plates with continuously varying thicknesses. A more advanced assumption is that thickness variation can be described using a normal distribution, as it is one of the most common distributions observed in various phenomena. However, while studies have shown that a normal distribution provides a reasonable approximation for thickness variation due to corrosion [29,30], this assumption can introduce errors in many real-world cases, as not all thickness changes strictly follow a normal distribution. For instance, pitting corrosion is better represented by an exponential distribution [30]. Furthermore, many natural processes involving thickness variations—both reduction and growth—do not follow a normal distribution. One such example is the formation of an additional ice layer on a surface. Although this system consists of multiple layers with variable thickness, its distribution is distinctly non-normal [31,32].

Since the development of a reliable, non-invasive method for assessing thickness variations remains a critical challenge in structural health monitoring, careful evaluation of the statistical assumptions regarding thickness distribution is essential—especially in cases where thickness variability cannot be easily described by a constant value or a normal or discrete distribution.

The aim of this study is to analyze wave propagation in plate-like structures whose shape is defined by sinusoidal functions [23]. The methodology for defining these geometries is detailed in the paper. However, their shape was specifically chosen to meet two key conditions. First, the thickness distribution of these plates is neither discrete nor normally distributed. Second, the primary focus is on examining how thickness variability affects wave propagation velocities. Despite using the same mathematical functions to describe the plate shapes, observable differences in wave propagation speed emerge, enabling a detailed analysis of the influence of thickness on wave behavior.

For each plate, the statistical parameters of the thickness distribution, namely the mean thickness and standard deviation, were known. The first step involved calculating dispersion curves for all tested plates and comparing them with theoretical predictions under two common assumptions:

- constant thickness approximation – assuming the plate can be successfully approximated as a uniform-thickness structure;
- normal distribution approximation – given that the two main statistical parameters (mean and standard deviation) are known, the thickness distribution is approximated using a normal distribution, which is a widely accepted assumption in similar studies.

A novel aspect of this work is the analysis of wave velocity variations for thickness distributions generated according to Chebyshev's theorem. Unlike normal distribution assumptions, Chebyshev's theorem is applicable to any distribution. Therefore, modeling thickness variation using Chebyshev's theorem provides a more generalized approach than assuming a specific, predefined distribution shape.

Finally, the study examines how different levels of complexity in modeling thickness distributions affect the solution of the inverse problem. This is done by progressively increasing the complexity of assumptions, from a constant thickness approximation to a normal distribution model, and then to a broader set of distributions generated according to Chebyshev's theorem. The outcome of this analysis is a set of statistical parameters describing the thickness distributions of the plates, determined using each of these approaches.

The paper is organized as follows: Section 2 provides an in-depth analysis of guided wave propagation in plates with variable thickness, discussing different statistical approaches to describe thickness variability. Section 3 presents the experimental and numerical methodologies used to validate the theoretical models. Section 4 contains the results, comparing wave velocity predictions under different thickness distribution assumptions and evaluating the accuracy of each approach. Finally, Section 5 discusses the implications of the findings and provides conclusions, along with potential directions for future research.

2. Guided wave propagation in irregular plates

In this section, the impact of thickness variability on wave propagation velocity is analyzed. The discussion begins with a general overview of the relationship between thickness and velocity. Subsequently, specific cases are addressed, including a normal distribution of thickness variability and a general distribution characterized using Chebyshev's theorem. The primary objective of this section is to highlight differences in wave propagation velocity resulting from various assumptions about the object's geometry. The analysis evaluates whether it is justified to approximate a plate with variable thickness as one with an averaged thickness or one whose thickness is described by a normal distribution.

2.1. The influence of thickness variability on wave propagation

The influence of thickness variability on wave propagation has been extensively studied in the literature. Since the propagation velocity of guided waves depends on plate thickness, the irregular geometry of a plate can cause the velocity to vary along the propagation path (Fig. 1).

Considering the distance from point A to B, the total time of flight (ToF) required to traverse this distance can be calculated as:

$$ToF(f) = \sum_{i=1}^{N} ToF_i(f) = \sum_{i=1}^{N} \frac{\Delta l_i}{c_{gi}(f)} \tag{1}$$

where N is the number of segments alongside the propagation path. If

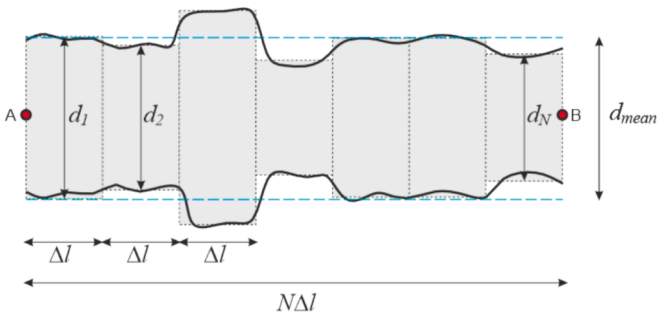

Fig. 1. Plate with irregular thickness.

the segment length Δl is constant, Eq. (2) can be rewritten as:

$$ToF(f) = \Delta l \cdot \sum_{i=1}^{N} \frac{1}{c_{gi}(f)} \tag{2}$$

where c_{gi} is the velocity determined for the plate thickness d_i. This approach to ToF estimation can be subject to inaccuracies, which depend on the lengths of segments Δl. The more the thickness is averaged, the greater the deviation between the estimated and actual time of flight. Based on the ToF, the velocity can be readily calculated:

$$c_{g,av}(f) = \frac{L}{ToF(f)} = \frac{L}{\Delta l \cdot \sum_{i=1}^{N} \frac{1}{c_{gi}(f)}} = \frac{N}{\sum_{i=1}^{N} \frac{1}{c_{gi}(f)}} \tag{3}$$

In general, the velocity described by Eq. (3) differs from the velocity, which is determined for a plate with a mean thickness d_{mean}. It should be noted, however, that the discrepancy between these velocities depends on the plate geometry—understood as the mean thickness and standard deviation of the thickness distribution—along with the material properties of the plate and the excitation frequency. In some cases, these differences are significant. However, there are situations in which approximating a plate with variable thickness as one with a uniform, averaged thickness is justified. These cases typically involve weakly dispersive modes, where the velocity remains constant or changes only slightly with varying plate thickness.

From Eqs. (2)–(3), it can be observed that the average velocity is not directly dependent on the exact plate geometry but rather on the thickness distribution along the propagation path. If the thickness distribution is known, it is possible to estimate both the average velocity and the total time of flight for a given excitation frequency.

2.2. Thickness variability defined by normal distribution

In many cases involving plates with irregular thickness, it is commonly assumed that the thickness distribution can be described using a normal distribution. There is also substantial evidence in the literature indicating that this type of distribution is typical, for example, in the case of general corrosion. General corrosion occurs over large areas, leading to gradual degradation of the plate and a reduction in its thickness. The general form of the normal distribution is expressed as:

$$f(x) = \frac{1}{\sigma\sqrt{2\pi}} e^{-\frac{1}{2}\left(\frac{x-\mu}{\sigma}\right)^2} \tag{4}$$

where μ denotes the mean, while σ is the standard deviation. In the considered case, the horizontal axis x represents the thickness, and the vertical axis represents the probability of its occurrence. To calculate the wave propagation velocity, the procedure of transforming the probability density function (PDF) into a histogram has been applied. Because the PDF is defined for variable x varying from $\pm\infty$, which has no physical sense if we consider real plates, it must be truncated first, as the thickness of the actual specimen varies from 0 to d, which denotes the thickness of the undamaged plate. The area under the curve f(x) has to be equal to 1 as it represents the probability, so after range modification, the area is determined and the truncated curve is scaled:

$$f_t'(x) = \frac{1}{Q} f_t(x) = \frac{1}{\int_0^{d_{max}} f_t(x)dx} f_t(x) \tag{5}$$

where $f_t(x)$ is truncated curve and $f_t'(x)$ is output scaled curve. In this way, we obtain a curve in a limited range corresponding to real plate thicknesses, and the area under it is again to 1 (Fig. 2b). To reconstruct the histogram from the PDF curve, first the bin width Δd has to be determined. Integrating over the range from d_i to $d_i + \Delta d$ gives the probability of the plate thickness falling within that range along a given propagation path of the selected length denoted as q_i:

$$q_i = \int_{d_i}^{d_i+\Delta d} f_t'(x)dx \tag{6}$$

The shape of the histogram depends on the number of measurement points i.e. how accurately the surface is reproduced. For example, if we measure the thickness along the propagation path with a step equal to 1 mm and the length of 100 cm, we obtain 1000 measurements, which are next used to create the histogram. To calculate the bin height n_i we can use the formula:

$$n_i = \frac{q_i L}{\Delta l} \tag{7}$$

where L is the total length of the propagation path, while Δl is the measurement step. The scheme of the procedure of transformation of normal distribution into histogram is presented in Fig. 2.

Based on the histogram and the derivations presented in Section 2.1 one can calculate wave propagation velocity measured on the distance characterized by variable thickness and defined by normal distribution. Fig. 2a presents the results in the form of averaged velocities calculated for the plates varying in mean thickness (from 5 mm to 10 mm) and for the frequency range up to 300 kHz but for a constant standard deviation equal to 2 mm. For comparison, the results for the plate with a constant thickness equal to the mean thickness have been added.

2.3. Chebyshev's theorem in thickness variability distribution

Chebyshev's theorem offers a powerful and distribution-independent framework for characterizing variability when only the mean and standard deviation of a dataset are known. Unlike methods that assume a specific probability distribution—such as the normal distribution—Chebyshev's theorem does not presume any particular shape of the distribution. This makes it especially well-suited for modeling complex and irregular thickness profiles, where the true distribution is unknown or clearly non-normal.

In guided wave propagation problems, the geometry of the medium (in this case, the thickness profile of a plate) plays a crucial role in determining wave velocity. Many practical scenarios, such as corrosion, material wear, or layered growth processes (e.g., ice accretion), lead to highly non-uniform and non-Gaussian thickness variations. Therefore, imposing a normal distribution assumption may not accurately capture these effects and can lead to significant prediction errors, especially in the estimation of wave velocity or structural integrity parameters like minimum thickness. Chebyshev's theorem provides a guaranteed bound on the proportion of data within a given number of standard deviations from the mean, regardless of the actual distribution. In general, there are two forms of the equation defined by Chebyshev. One determines how close to the mean the data lie and the other calculates how far away from the mean they fall. The first one defines the minimum proportion of observations that are within k_c standard deviations of the mean:

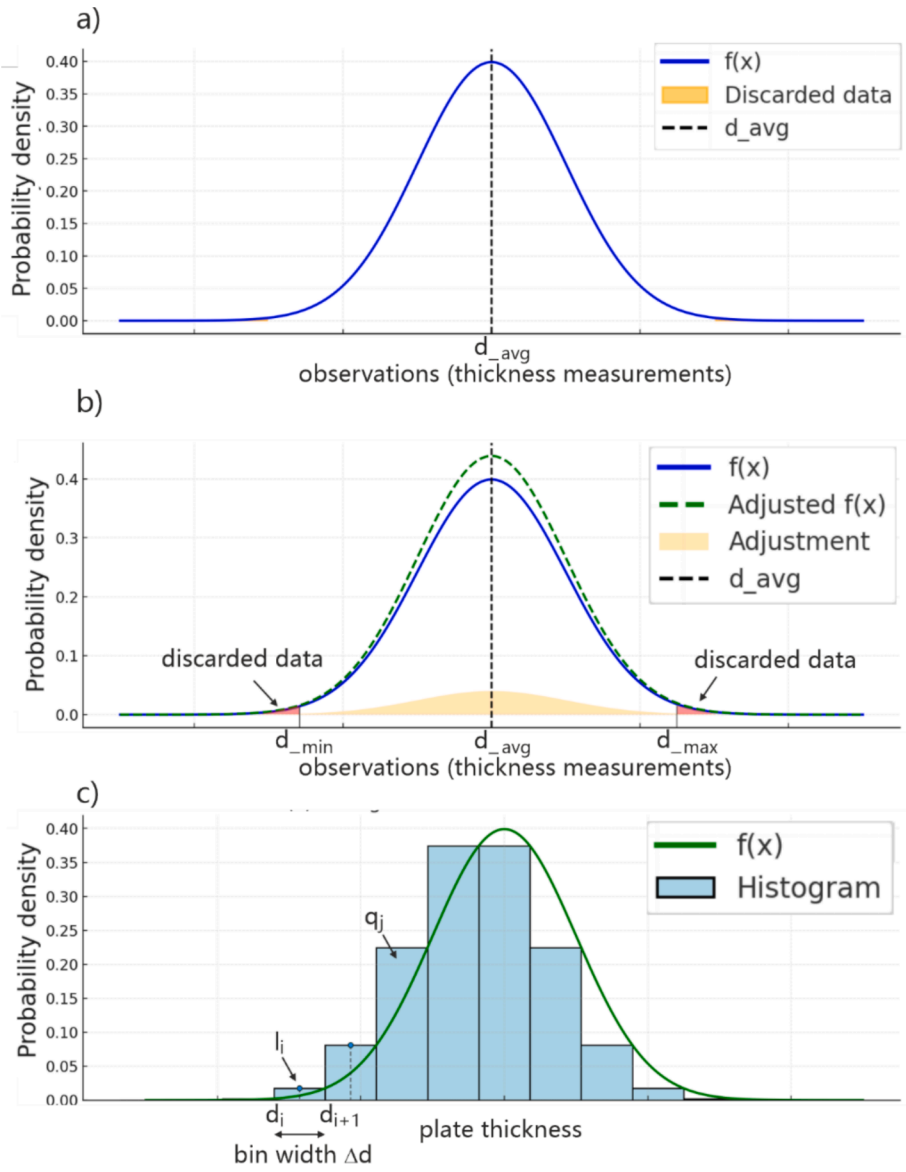

Fig. 2. Schematic representation of the transformation process from a normal probability density function (PDF) to a histogram of thickness distribution: a) normal distribution, b) discarded data above and below certain limit values and c) transformation into histogram (description of the transformation procedure is given in the text).

$$1 - \frac{1}{k_c^2} \tag{8}$$

where k equals the number of standard deviations and it must be higher than $\pm$ 1. The second one defines the maximum proportion of observations that are more than k_c standard deviations from the mean:

$$\frac{1}{k_c^2} \tag{9}$$

In the further part of the paper we will mainly use Eq. (8). A crucial point to notice is that Chebyshev's theorem produces minimum and maximum proportions. This inequality implies that at least $1 - \frac{1}{k_c^2}$ of the data lies within k_c standard deviations of the mean, even if the actual distribution is skewed, multimodal, or otherwise non-normal.

In this study, the Chebyshev theorem is applied to generate thickness distributions using only the mean and standard deviation as input parameters. A MATLAB script was developed to generate these distributions, following the steps outlined below:

1. Define the mean value and the number of standard deviations. In this case, we considered distributions spanning the range from -5 to $+5$ standard deviations.
2. Calculate a Chebyshev-like sequence for the vector k_c using the formula from Eq. (8). This determines the percentage of results that should fall within each interval.
3. Using these proportions, the script randomly generates samples within the defined intervals, ensuring consistency with the percentages determined in the previous step.
4. Once all samples are assigned to the respective intervals, a histogram of the thickness distribution is created.
5. The wave velocity is calculated according to the procedure described in Section 2.1 based on the histogram (i.e., the length of the path characterized by a given thickness).

This method offers a generalized and flexible alternative to the normal distribution model, allowing for a broader and more realistic representation of the thickness variability observed in physical specimens. It is especially advantageous when the underlying distribution is

unknown, non-symmetric, or influenced by localized damage mechanisms (e.g., pitting).

Fig. 3 shows three example distributions characterized by the same mean and standard deviation (mean of 5 and standard deviation of 2), generated according to Chebyshev's theorem. As can be seen, each distribution differs from the others despite having identical parameters. The clustering of sample values in the central part of the distributions is due to the relatively small standard deviation, which is five times smaller than the mean.

2.4. Comparison of theoretical predictions regarding wave velocity in plates with variable thickness

To compare the results obtained under different assumptions regarding thickness distributions, the following analysis was performed: normal distributions and distributions that satisfied the conditions of Chebyshev's theorem (but were not normal distributions) were generated, and their guided wave group velocities were determined according to the method described in Section 2.1. Additionally, given that distributions generated according to Chebyshev's theorem differ from one another, the wave velocity for these distributions was calcula3ed based on 100 generated distributions with identical statistical parameters and then averaged. Moreover, for each case, the wave velocity was also calculated for a plate with a constant, average thickness, i.e., without considering the possibility of variable thickness. The results for selected parameters are presented in Fig. 4. The calculations were performed for an aluminum plate with the same parameters as the plates described later in this study. The dispersion curves were generated in the fd range from 0 to 1000 kHz x mm for the variable standard deviation, which was equal to 1 mm, 2 mm, 5 mm, and 10 mm. The considered standard deviations may be relatively large, but the goal was not to analyze a specific real-world case but rather to illustrate a general trend. When the standard deviation is small and the plate thickness is concentrated close to the mean thickness then the differences in velocities obtained in different ways are similar. However, the increase in the thickness distribution causes the differences between velocities to reach even more than 1000 m/s, which is more than 30 % of the actual result (see Fig. 4d).

3. Materials and methods

3.1. Experimental models

In this study, plates with one flat surface and one surface described by a sine function were selected for analysis. This design was chosen due to its ability to introduce controlled thickness variability while avoiding undesired effects caused by abrupt thickness changes, as seen in stepped plates. The smooth sine shape allowed for a systematic investigation of the influence of thickness variation on wave propagation characteristics, ensuring accurate and interpretable results. The equation governing the upper surface of the plate is:

$$s(x) = A \cdot \sin(kx - \varphi) + h_0 \tag{10}$$

where A is the amplitude, k is the wavenumber, φ is the phase shift, and h_0 is the initial thickness of the plate. These parameters were chosen considering their impact on wave velocity differences among the plates, as well as practical factors such as manufacturing capabilities, costs, and safety. The goal was to ensure that variations in time-of-flight (ToF) would be measurable while maintaining safe and efficient manufacturing processes. The sine-shaped surface offered several advantages. The smooth transition instead of tapered abrupt thickness changes reduced unwanted reflections and mode conversions triggered by sharp transitions, simplifying the interpretation of wave behavior. By adjusting parameters such as amplitude, wavenumber, and phase shift the geometry of the plate could be precisely tailored to maximize differences in wave velocity across plates. Additionally, the histogram of thickness distribution for a sine-shaped plate is more suitable for the conducted analysis compared to stepped plates because it contains more thicknesses, facilitating the analysis of wave propagation phenomena.

Several factors dictated the detailed explanation of the selected shape. The plates were fabricated using a specialized CNC milling machine, each with a total length (L) of 400 mm and a width (W) of 250 mm. The initial thickness, $h_0 = 10$ mm, was selected to balance the mass required for safer manufacturing and the theoretical ToF variations (which increase with thinner cross-sections). In general, for plates with greater thickness (higher fd product), the dispersion curve for the A0 mode becomes flat. This implies that variations in thickness do not significantly affect wave speed, or the differences are so negligible that results obtained for various plates would not diverge sufficiently to draw meaningful conclusions. Conversely, thinner plates result in a lower overall mass, which introduces challenges during CNC machining. Lightweight components are more prone to vibrations, leading to reduced manufacturing accuracy. The thickness of ho = 10 mm was deemed a practical compromise between the goal of investigating thinner plates and the technological limitations of the available equipment.

To determine the values of the remaining parameters describing the plate shape (A, k, and φ), the following assumptions were made: the parameters A, k, and h_0 were kept constant for all manufactured plates, with the only variable being the phase shift φ. Additionally, it was assumed that the number of plates to be studied would be four, a choice further elaborated later in this section. Constraints were then established for the phase shift values. Extreme values were selected to ensure the greatest differences in plate thicknesses, which, in turn, were expected to result in the most pronounced changes in wave velocity. Notably, selecting $\varphi_1 = 0$ and $\varphi_4 = \pi$ led to one plate being convex while the other was concave, yielding the most significant velocity differences as predicted by theoretical models. The two remaining plates were designed under the assumption that the phase shift increment would remain constant at $1/3\pi$. Ultimately, four distinct plates with varying phase shifts ($\varphi_1 = 0$, $\varphi_2 = 1/3\pi$, $\varphi_3 = 2/3\pi$, $\varphi_4 = \pi$) were selected to investigate the effects of convex, concave, and intermediate shapes on wave velocity.

The parameters A and k were selected based on the results of the analysis presented in Fig. 5. This analysis concerns the theoretical average velocity of the A0 mode, measured over a segment equal to the plate length, for varying parameters A and k. Each row represents results for a selected frequency, ranging from 100 to 300 kHz. The left column

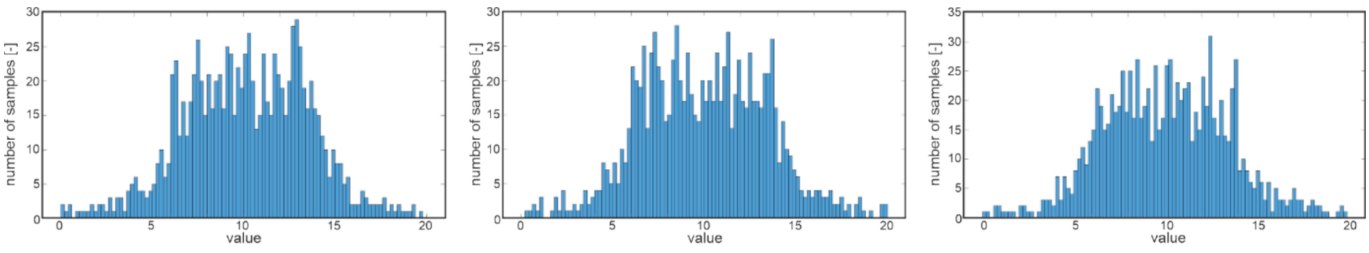

Fig. 3. Three different distributions generated according to the described procedure for the mean value of 10 and the standard deviation of 2.

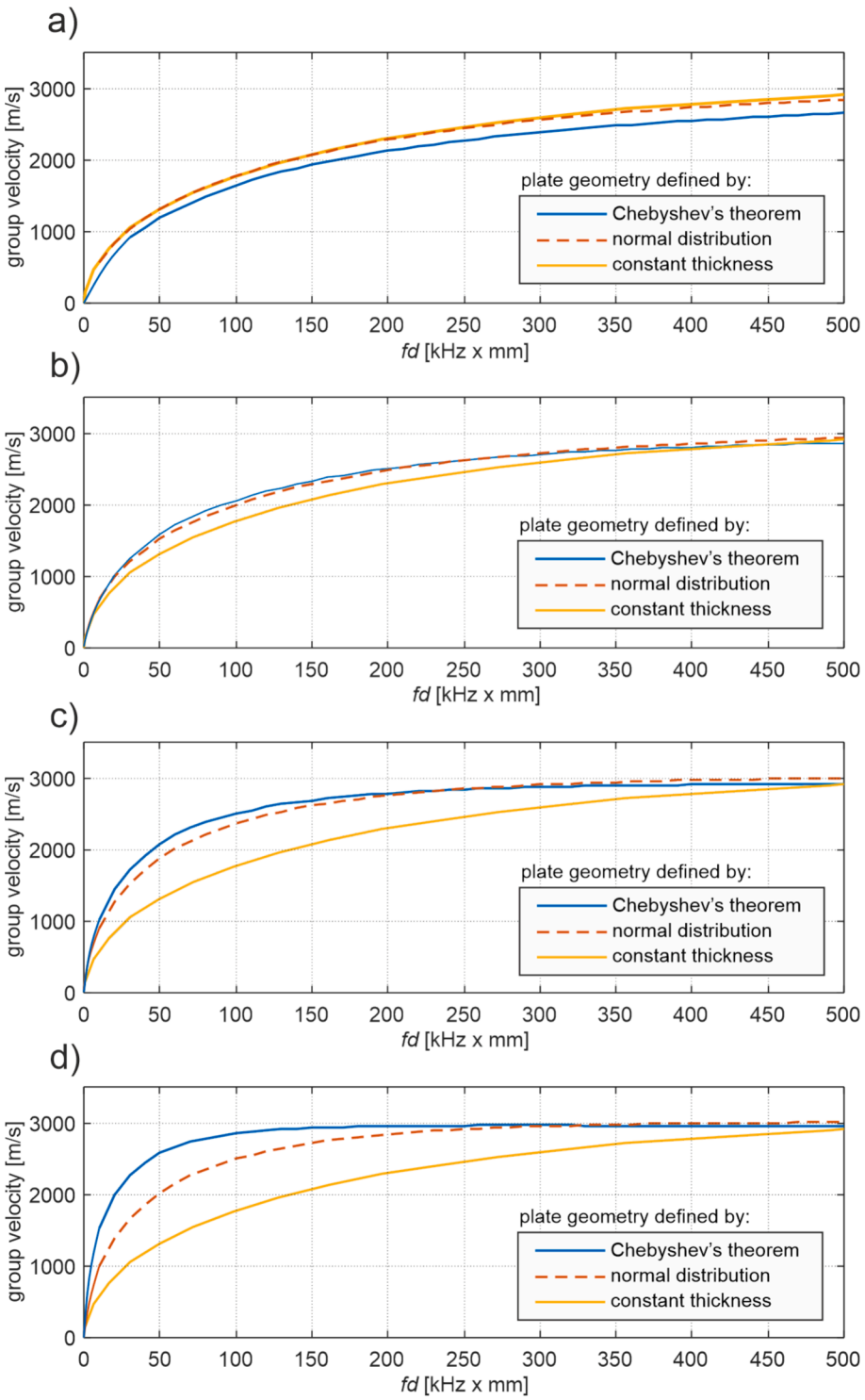

Fig. 4. Comparison of guided wave group velocities for different thickness distribution assumptions. The dispersion curves were generated for the aluminum plates with the thicknesses described by normal distributions, distributions generated according to Chebyshev's theorem, and a constant thickness approximation and for variable standard deviation equal to: a) 1 mm, b) 2 mm, c) 5 mm and d) 10 mm.

shows results for a constant $k = 0.01$, while the right column displays results for a variable wavenumber k but with a constant amplitude $A = 7$ mm.

The results indicate that the interaction between wave velocity, plate geometry, and frequency is highly non-linear and challenging to predict. Maximizing velocity differences at one frequency does not necessarily extend to the entire frequency range. The final parameters for the four plates are indicated by black dots in the figures. For example, based on results obtained at 100 kHz, it can be inferred that the velocity differences between the plates increase with higher amplitude A. However, at higher frequencies, this conclusion is not valid. Ultimately, the amplitude A was selected under the assumption that the tests would be conducted in the lower frequency range. Therefore, A should be as high as possible, but its upper limit was constrained by previously mentioned safety considerations for sample fabrication. A higher amplitude corresponds to a thinner plate in its thinnest cross-section, which negatively

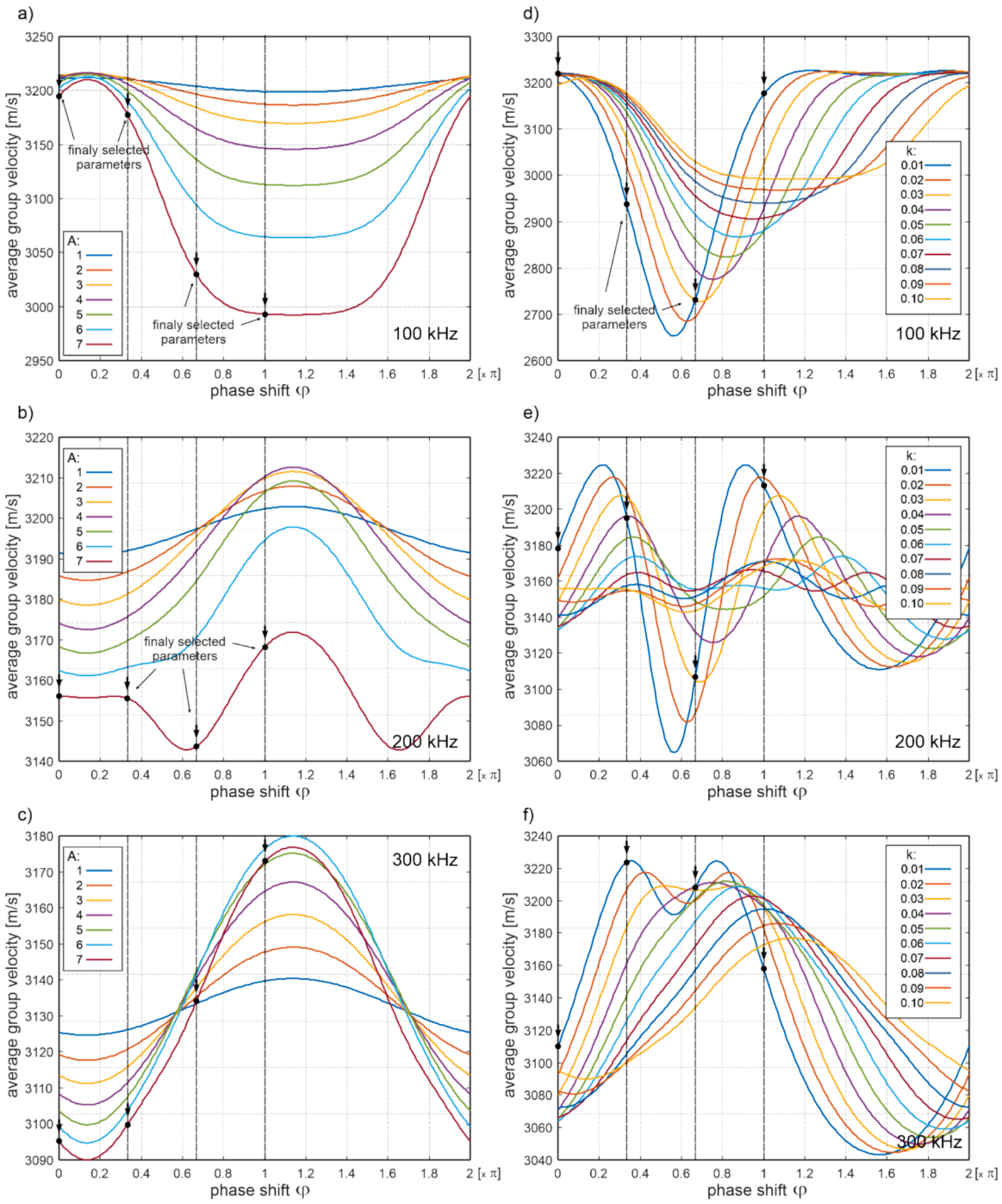

Fig. 5. Selection of parameters A (amplitude), k (wavenumber), and φ (phase shift) for the investigated plates. The average group velocity for constant $k = 0.01$ (left column) and variable amplitude and constant amplitude $A = 7$ (right column) and for variable k (results at a) and d) are for 100 kHz, b) and e) 200 kHz and c) and f) 300 kHz).

impacts the quality of sample production. Ultimately, the amplitude was set at 7 mm.

A similar analysis was performed for the wavenumber k (right column). As seen, for instance, at 100 kHz, the differences increase as k decreases. With increasing wavelength, the wavelength becomes relatively longer compared to the plate's dimensions, and the plate thickness exhibits less variability. However, the analysis showed that the greatest velocity differences occurred at different excitation frequencies for plates of different shapes. As a result, analyzing this issue is not straightforward.

Finally, the function describing the upper plate surface has taken the following form:

$$s(x) = 7 \cdot \sin(0.01x - \varphi) + 10[\text{mm}] \tag{11}$$

Fig. 6 illustrates the geometry of the plates along with histograms representing the thickness distributions. These histograms were generated using thickness measurements taken at increments of 10^{-3}, with the results organized into 100 bins. The vertical axis of each histogram reflects the frequency at which specific thicknesses appear in the cross-sections. The obtained histograms do not follow a normal distribution. Instead, the thickness variations resemble an exponential distribution, with peaks shifted toward the extreme values of plate thicknesses.

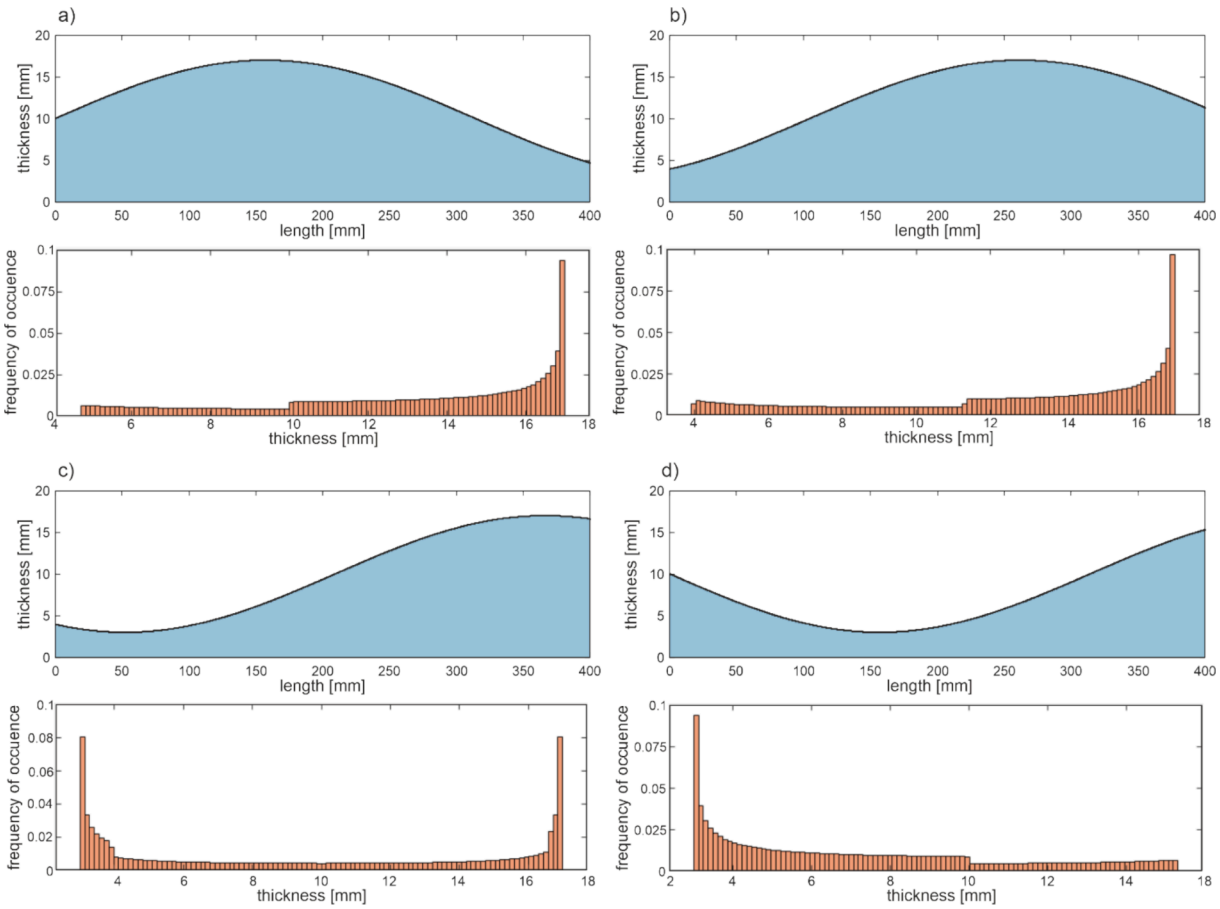

Fig. 6. Geometry of the investigated sinusoidal plates along with corresponding thickness histograms: a) plate #1, b) plate #2, c) plate #3 and d) plate #4.

The sinusoidal plates used in this study were intentionally selected because they provide a controlled and repeatable method of introducing thickness variability. By defining plate geometry using the same sinusoidal function and altering only the phase shift parameter, it was possible to generate a diverse set of thickness distributions while maintaining consistent fabrication precision. Importantly, the sinusoidal shape ensured that the resulting distributions deviate from the normal form, which was a key requirement for evaluating the effectiveness of Chebyshev's theorem. This setup allowed for a clear demonstration of the limitations of assuming either a constant average thickness or a normal distribution, both of which introduce inaccuracies when modeling wave propagation in plates with non-uniform geometry.

The subsequent sections of this work will focus on analyzing the extent of errors in wave velocity estimation when these assumptions are applied and whether their use is justifiable. The actual experimental objects, manufactured using a CNC machine, are shown in Fig. 7.

3.2. *Experimental equipment*

Guided waves in this study were actuated and detected using rectangular piezoceramic transducers measuring 30 × 5 mm, supplied by Physik Instrumente. These transducers were selected for their ability to produce a straight wavefront, which minimizes inaccuracies in time-of-flight (ToF) measurements that could result from circular wavefront propagation. To ensure accurate and perpendicular excitation, the transducers were adhered to the flat side of the plates.

The wave signals were generated and recorded using a Handyscope HS5 oscilloscope and function generator from TiePie Engineering. To enhance the signal-to-noise ratio, the receiving transducer was connected to a high-voltage amplifier (PD200, PiezoDrive Ltd, Shortland,

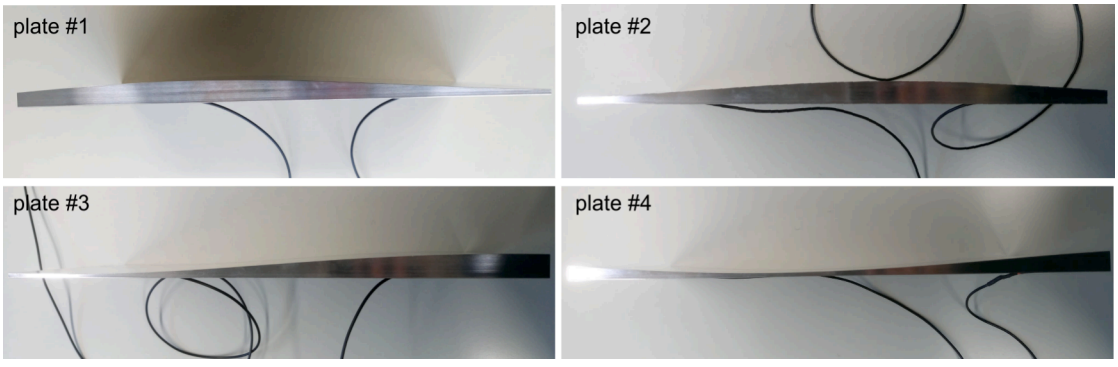

Fig. 7. The photos of investigated plates.

NSW 2307, Australia). The amplified signals were then transmitted to a custom-built device named Rammsbone, described comprehensively in [33].

The excitation signal was defined as a five-cycle sine wave modulated by a Hann window. Measurements were conducted for frequencies ranging from 150 kHz to 300 kHz, with 10 kHz increments, resulting in a total of 16 carrier frequencies used throughout the testing.

3.3. Measurement inaccuracies

The study involves measuring wave velocity, which varies along the length of the plate. This velocity is influenced not only by the plate's geometric and material properties but also by measurement inaccuracies. For clarity and completeness, the specific uncertainties associated with the experimental models and the measurement equipment used in the study are presented below.

The primary sources of measurement inaccuracy included plate thickness measurements, ToF extraction, and wave velocity estimation. Thickness measurements were carried out using a micrometer with a resolution of 0.01 mm, as specified by the manufacturer. Multiple measurements were taken across each plate surface to account for local variability and improve statistical confidence.

ToFs values were extracted from guided wave signals. The uncertainty in ToF was primarily influenced by signal interpretation and time resolution. Given the sampling rate of 10 MHz and the applied signal filtering, the ToF uncertainty was estimated to be within $\pm$ 0.1 μs.

Wave velocity estimation was affected by uncertainties in both ToF and the transducer spacing. The transducers were mounted with care to minimize misalignment. The distance between them was measured using a standard tape measure, with an estimated measurement uncertainty of $\pm$ 1.2 times the smallest division (0.5 mm), in accordance with standard metrology guidelines.

3.4. Numerical models

The numerical plate models were created using the commercial software Abaqus. The Dynamic/Explicit module was employed to simulate the propagation of mechanical guided waves accurately. Three-dimensional models were constructed using eight-node brick elements with reduced integration (C3D8R). The transient wave propagation problem was solved with a time step of 10^{-7} s, determined based on the Courant–Friedrichs–Lewy condition. Prior to setting the finite element size, a convergence study was conducted to ensure accuracy. The element dimensions were restricted to a maximum of 1 mm^3. The excitation was implemented as a time-dependent pressure applied over an area corresponding to the actual piezoelectric transducers used in the experiments. A numerical model incorporating this pressure application is shown in Fig. 8. The excitation waveform was a five-cycle sine function modulated by a Hann window, expressed as:

$$p(t)\begin{cases} 0.5p_0\sin\left(2\pi ft\left(1-\cos\left(\frac{2\pi ft}{n_w}\right)\right)\right), & t\in[0,T_w] \\ 0t \geq T_w \end{cases} \tag{12}$$

where f represents the excitation frequency, t denotes time, p_0 is the amplitude, T_w denotes the Hann window duration, and n_w corresponds to the number of time steps.

The material properties used in the model were as follows: Young's modulus $E = 70$ GPa, Poisson's ratio $\nu = 0.33$, and density $\rho = 2700$ kg/m^3. The simulations were performed using a 3D model because a plane strain approximation would not allow for the realistic application of excitation over the actuator area. Furthermore, the 3D model enables the observation of boundary reflections present in experimental conditions, thereby offering a more accurate representation of the physical system. The validity of the numerical simulations was confirmed by comparing the results with experimental data, as detailed in a subsequent section of this paper.

4. Results

Fig. 9 presents the results in the form of time-domain signals recorded for all plates. To ensure readability, results are shown for only three selected frequencies. As observed, both the ToF and the signal characteristics vary for each plate. These differences are evident not only between the plates but also in the time-domain waveforms obtained from the experimental and numerical analyses.

The discrepancy in signal waveforms is primarily due to the idealized nature of the numerically analyzed plates. In the numerical models, the transducer was placed perfectly at the center, applying uniform pressure to the plate and generating a wave under ideal conditions. The adhesive layer was omitted in the numerical model, resulting in the excitation being applied perfectly perpendicular to the flat surface of the plate.

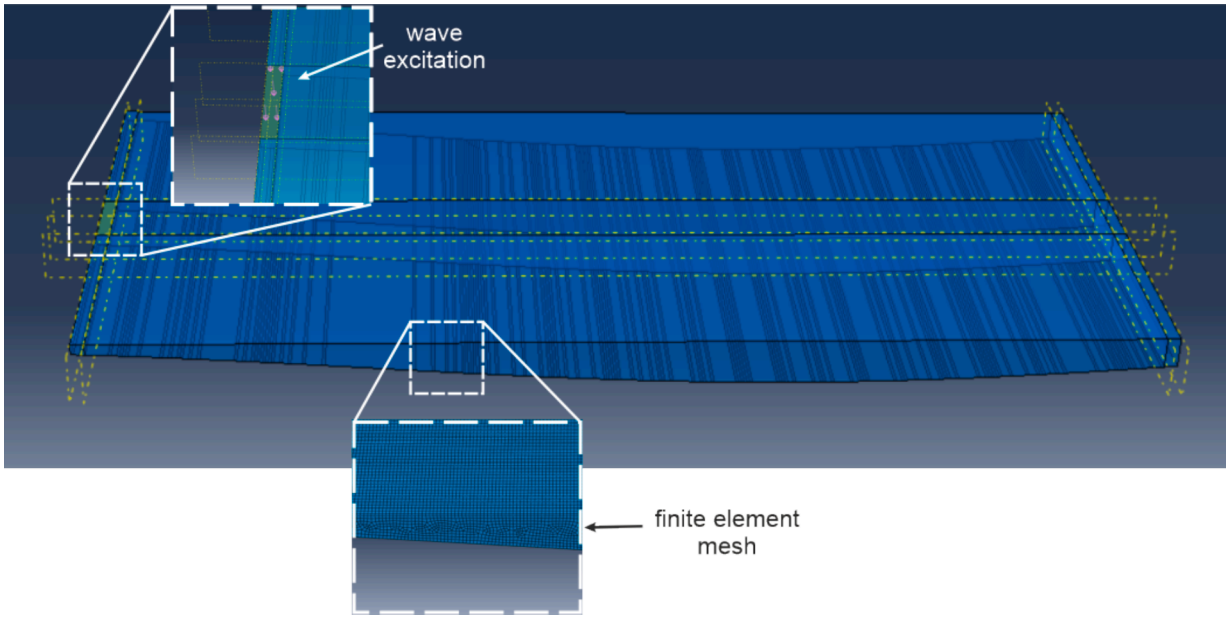

Fig. 8. The numerical model of the one of considered plates (plate #1).

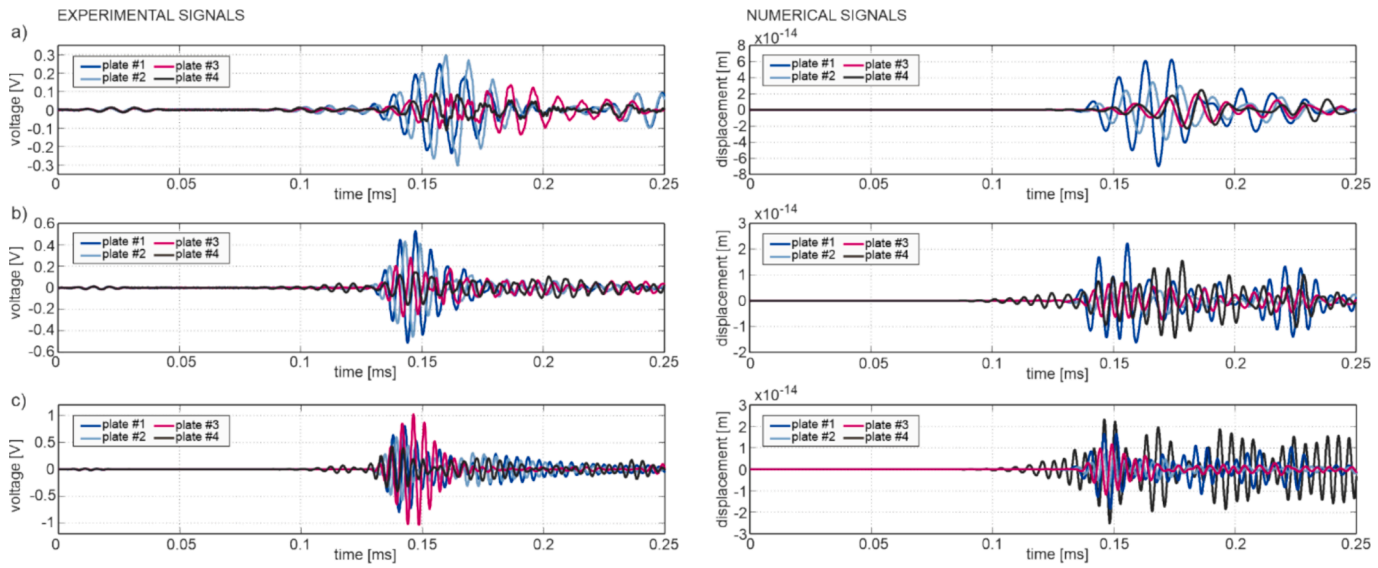

Fig. 9. Experimental (left column) and numerical (right column) time-domain signals of guided waves recorded for all tested plates at selected frequencies: a) 100 kHz, b) 150 kHz and c) 200 kHz.

Waves propagating along the plate and reflecting from its edges produced a perfectly symmetrical pattern, with reflections occurring simultaneously and interfering with one another.

In contrast, for the experimental model, despite being meticulously prepared from metal with the highest precision, minor material and geometric imperfections cannot be excluded. However, the primary factor contributing to the differences between numerical and experimental results was the non-ideal placement of the transducer. Firstly, even with the use of a thin adhesive layer, the possibility of non-perpendicular transducer attachment cannot be ruled out. This could

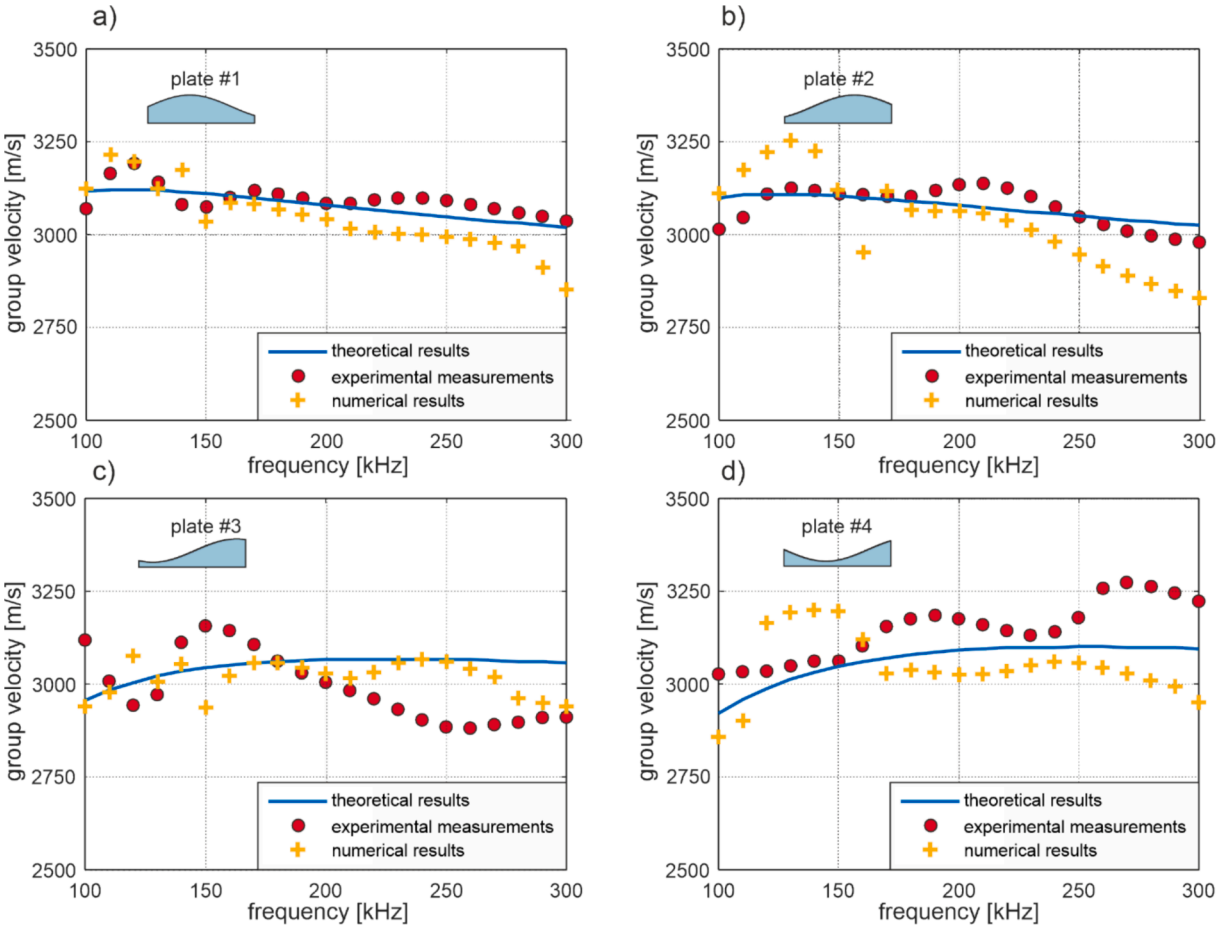

Fig. 10. Comparison of dispersion curves obtained from experimental, numerical, and theoretical predictions under different thickness distribution assumptions: a) plate #1, b) plate #2, c) plate #3 and d) plate #4.

lead to the excitation of not only the antisymmetric mode but also symmetric modes. Additionally, any misalignment or rotation of the transducer relative to the plate's symmetry axis could disrupt the symmetry of the propagating wavefield. Consequently, reflections from the edges could become temporally shifted relative to one another, significantly altering the recorded time-domain signals and their characteristics.

Despite the noticeable differences in the time-domain waveforms, the most important observation is the consistency of the ToF for the first wave packet recorded at the opposite end of the plate (Fig. 10). Moreover, the order of the recorded signals for the individual plates clearly reflects differences in the average wave velocities caused by the variable thickness. Since the time of flight is the key parameter analyzed in the subsequent sections of this study, the obtained results can be considered valid and suitable for further analysis. Fig. 10 also illustrates the consistency of the flight time, which compares numerical, experimental, and theoretical results calculated using the procedure described in Section 2.

4.1. Theoretical predictions of the wave propagation velocity

To determine the theoretical wave velocities for the A0 mode, the average thickness and basic statistical parameters, such as the mean thickness and standard deviation, were calculated for each plate (Table 1).

Subsequently, the velocities were determined under the following assumptions: (I) for a constant, average thickness; (II) for a scenario where the thickness distribution is not constant but can be approximated by a normal distribution; and (III) for a case where the distribution is not precisely known but satisfies the conditions of Chebyshev's theorem. In the final step, (IV) the theoretical velocity was calculated based on the actual distribution, as represented in Fig. 6. The results, in the form of dispersion curves, are presented in Fig. 11. Additionally, the representative results obtained from the experimental campaign have also been added to the figure.

A visual assessment of the obtained results indicates that, regardless of the assumptions made about the thickness distributions of the plates, the relationship between velocity and frequency within the analyzed range closely corresponds to the experimental results. To quantitatively evaluate the results, the mean square error (MSE) was calculated between the experimental data and the theoretical predictions derived for different thickness distributions.

The results are presented in a table and in Fig. 12. The findings indicate that the smallest errors, regardless of the approach used to calculate wave velocity, were obtained for plates #1 and #2. These errors are significantly lower—by several times—compared to those for plates #3 and #4. The main reason for these differences is likely the nature of the thickness variability. Plates #1 and #2 exhibit the highest average thickness (over 12 mm). Moreover, the variability of the thickness distribution is less pronounced compared to plates #3 and #4: the standard deviations for plates #1 and #2 are 28 % and 33 % of the average thickness, respectively, while for plates #3 and #4, they are 56 % and 51 %. This means that the thickness distributions for plates #1 and #2 are more concentrated around their mean values. Additionally, this concentration occurs around a relatively high value of approximately 12 mm. For such thicknesses, the dispersion curve for the A0 mode flattens, which reduces the impact of thickness variations on wave velocity. Therefore, the results obtained for plates #1 and #2 can be considered sufficiently accurate, even when the plate shape is approximated by a constant thickness.

Table 1
Statistical parameters describing thickness variability of the considered plates.

specimen	mean thickness [mm]	standard deviation [mm]
plate #1	12.894	3.619
plate #2	12.294	4.031
plate #3	9.700	5.382
plate #4	7.106	3.619

A second observation from the results concerns the relationship between the error magnitude and the method used to estimate wave velocity. While this observation is specific to the analyzed sinusoidal plates, it is evident that relatively small errors were obtained when the exact thickness distribution was known, allowing for accurate theoretical velocity determination. In three out of the four cases analyzed, the values derived from the exact distribution (Fig. 6) yielded the lowest errors.

In contrast, the largest errors were consistently observed when it was assumed that the distribution of thickness could be approximated as normal, based on its mean and standard deviation. This assumption even resulted in slightly larger errors than assuming a constant plate thickness. This discrepancy can be explained by examining the actual thickness distributions, which are far from normal. The maximum values occur at the extreme thicknesses, whereas the mean thickness—associated with the highest probability in a normal distribution—appears relatively rarely in the analyzed plates. This example highlights that abandoning simplifications in favor of more complex but incorrect assumptions about the distribution's nature can worsen the results.

Another notable observation pertains to estimating theoretical velocity using Chebyshev's theorem. In all cases, the error obtained with this assumption was lower than that from assuming a normal distribution. In three out of four cases, the error using Chebyshev's theorem was also lower or comparable to the assumption of constant thickness (and consequently constant velocity). Using Chebyshev's theorem to generate a distribution based on the mean and standard deviation resulted in slightly higher errors compared to predictions based on the exact thickness distribution. Based on these results, it can be inferred that applying Chebyshev's theorem, particularly when the exact nature of the thickness distribution is unknown, leads to better results than assuming either constant thickness or a standard normal distribution.

The only exception to the above trends was observed for plate #4. For this plate, the best result was obtained using the simplified assumption of constant thickness. Comparing the experimentally obtained results reveals that they do not follow a consistent trend; instead, the function exhibits local increases and decreases.

In general, it is important to note that the experimental results may not perfectly match the theoretical predictions for several reasons. First, the Lamb wave dispersion equations are derived for a two-dimensional plane-strain plate model. These equations were used in this study to calculate the theoretical wave propagation velocity. In reality, the emitted primary waves interact with their reflections from the plate's side edges, resulting in complex wave patterns that complicate signal interpretation. Furthermore, symmetric modes are also triggered and overlap with antisymmetric modes.

Second, the nature of the experimental dispersion curves must be considered in the context of the influence of plate shape and the potential presence of evanescent modes. Beyond the thickness cut-off, the adiabatic mode may reflect or convert into a different guided wave. Therefore, the concave shape and decreasing thickness of plate #4 likely influenced the observed wave propagation phenomena.

Third, the complexity of the phenomenon is strongly dependent on the thickness distribution, which can induce or suppress certain Lamb modes. To aid in interpreting these effects, Fig. 13 presents four sets of dispersion curves, one for each plate. Each plot highlights a specific range. The lower boundary of this range was determined by calculating the *fd* product for the lowest frequency used in the study (100 kHz) and the smallest thickness for the given plate. Similarly, the upper boundary was calculated for the maximum frequency (300 kHz) and the largest thickness. All modes occurring within this range could potentially be excited during wave propagation in the respective plate. To assess the potential excitation of higher-order modes, wave propagation at the maximum operating frequency of 300 kHz was considered. As the plate

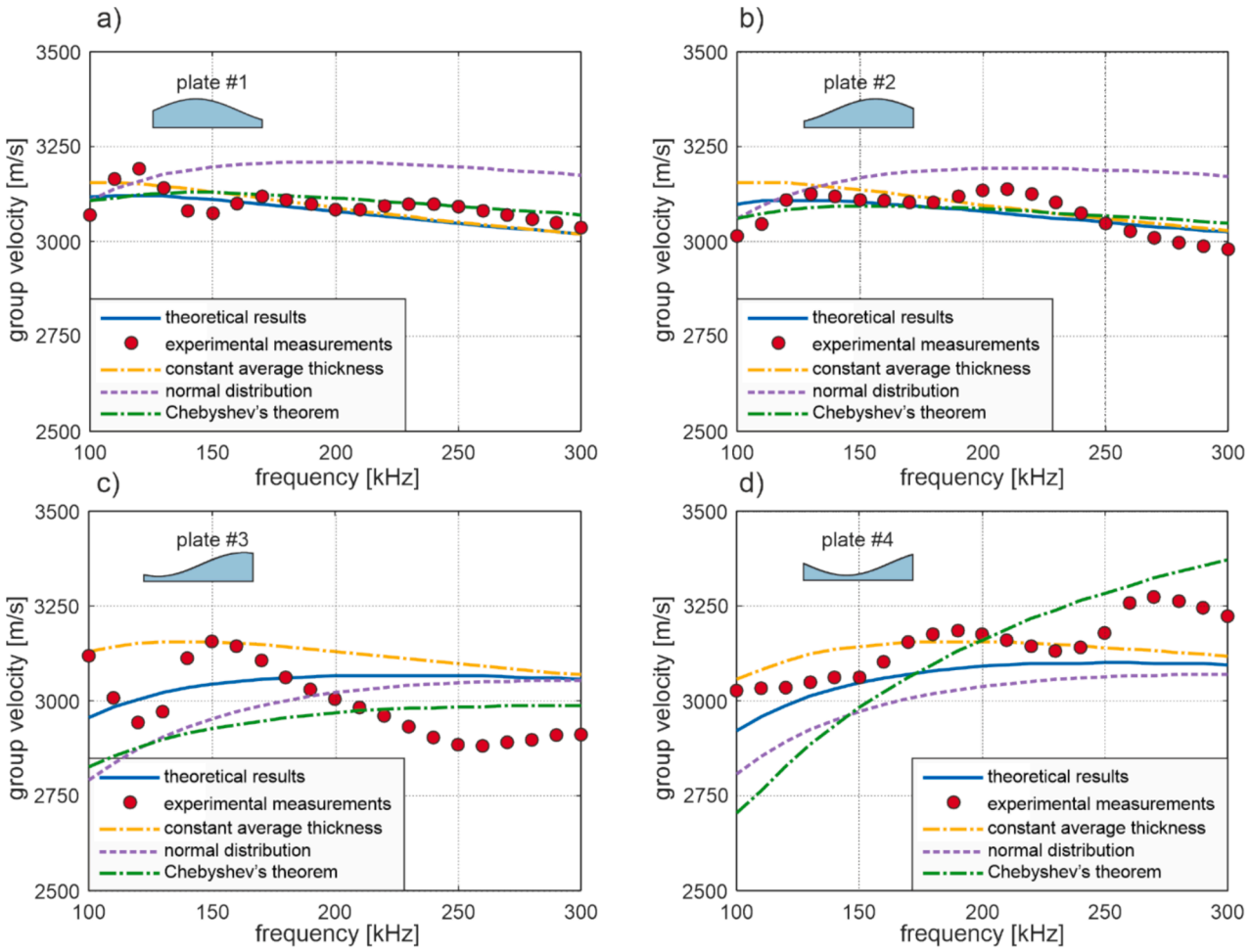

Fig. 11. The dispersion curves determined based on different thickness distributions generated for the statistical parameters (mean and the deviation) of the actual plates for a) plate #1, b) plate #2, c) plate #3 and d) plate #4.

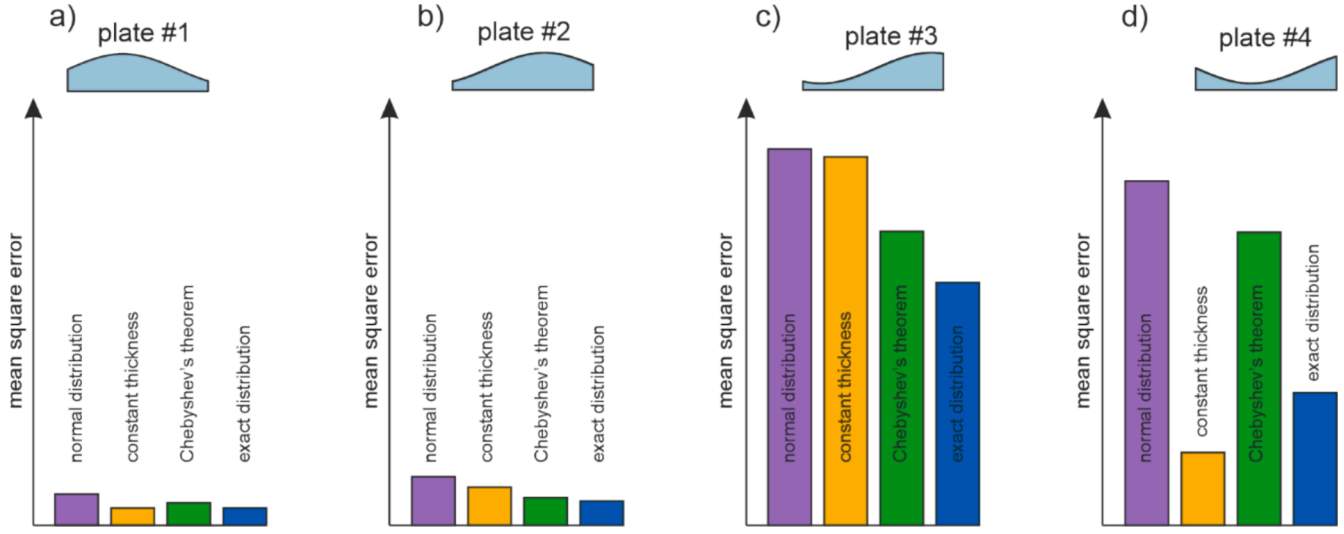

Fig. 12. Mean square error (MSE) between experimental and theoretical wave velocities under different thickness modeling assumptions: a) plate #1, b) plate #2, c) plate #3 and d) plate #4.

thickness decreases, higher-order modes tend to reflect and either travel back along the structure or undergo conversion into fundamental lower-order modes [19,21]. A comprehensive mode conversion analysis was carried out for all plate samples. In every case, it was determined that only the fundamental S0 and A0 modes could propagate across the entire length of the plates. As a result, the subsequent investigation focused primarily on these two modes.

From the perspective of the obtained results, a significant

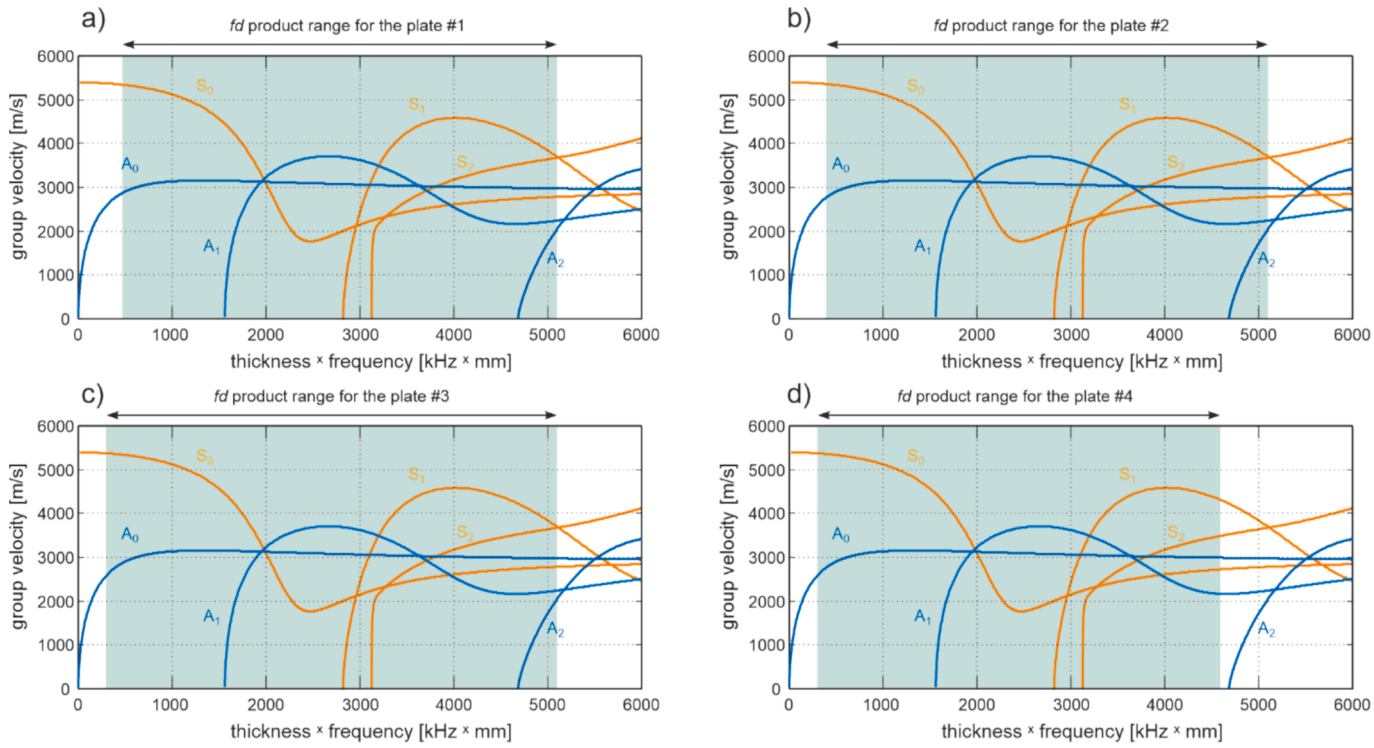

Fig. 13. Determination of the *fd* product range and wave modes which can occur in a) plate #1, b) plate #2, c) plate #3, d) plate #4 for excitation frequency of 100 kHz to 300 kHz.

observation is that the highlighted regions for plates #3 and #4 begin earlier (at lower *fd* product) than for plates #1 and #2. Consequently, these regions encompass a larger portion of the A0 mode curve, which was primarily triggered during the experimental campaign. The A0 mode curve is characterized by a steeper slope and is therefore more sensitive to changes in plate thickness. This may explain why the errors obtained for plates #3 and #4 were higher than those for plates #1 and #2.

4.2. Determination of the geometric parameters based on wave propagation signals

The final stage of the study involved solving the inverse problem, i.e., attempting to determine the statistical parameters of the thickness distribution based on the obtained results. To achieve this, the following steps were carried out:

1. Dispersion curves were generated for various thicknesses.
2. Normal distributions were generated with mean values ranging from 3 mm to 30 mm and standard deviations from 0.5 mm to 10 mm. The propagation velocity was calculated for each distribution.
3. Thickness distributions were generated according to Chebyshev's theorem, using the same parameter ranges (mean values from 3 mm to 30 mm and standard deviations from 0.5 mm to 10 mm). For each set of parameters, 10 different distributions were generated, the wave velocity was calculated, and the results were averaged.
4. In the final step, the obtained results were compared with the experimental data by calculating the following value:

$$\min\left(\frac{1}{N}\sum_{i=1}^{N}\left|c_{gt}-c_{ge}\right|^{2}\right) \tag{13}$$

Here, c_{gt} represents the theoretical group velocity in the form of an N-element vector calculated as described in steps 1–3, while c_{ge} represents the experimentally determined group velocity. The minimum value of this expression described by Eq. (13) corresponded to the best fit between theoretical and experimental results.

The results of this analysis are summarized in Tables 2 and 3. Table 2 contains a summary of the experimental results, while Table 3 presents the outcomes from numerical analyses. Both tables include information on the mean thickness and standard deviation determined using the approach described above. Additionally, the relative error for each result was calculated and expressed as a percentage. Both tables highlight key results: the smallest errors for mean thickness are shaded in gray, while the smallest errors for standard deviation are highlighted in green.

For the experimental results, the best matches were obtained using different approaches, depending on the plate. For example, in the case of plate #4, the best thickness estimation was achieved using the simplest approach, which assumes the plate can be described by a constant mean thickness. However, in the remaining cases, more complex assumptions about the thickness distribution provided significantly better matches. In particular, distributions generated using Chebyshev's theorem resulted in better approximations of both the mean thickness and standard deviation.

When using a normal distribution, the best match for mean thickness was achieved in one case (plate #1), while the standard deviation was determined with a small error (approximately 2 %) in two cases (plates #2 and #3). On the other hand, the application of Chebyshev's theorem produced the best mean thickness estimations in two cases (plates #2 and #3), while the standard deviation was determined with high accuracy (error around 3 %) in three cases (plates #1, #3, and #4).

The advantage of using Chebyshev's theorem, which provides proportional results without assuming an exact distribution shape, was even more pronounced for the numerical results. In two cases, thickness estimation using this method yielded the best match, while for standard deviation, the best result was obtained in three cases. Notably, the error in estimating the standard deviation was less than 6 % in every instance. The estimation of mean thickness also demonstrated reasonable accuracy, with errors below 30 % in all cases. Moreover, in three cases, the

Table 2
Comparison of exact and estimated parameters based on experimental results under different assumptions about thickness distribution.

	exact statistic parameters		assumption of average, constant thickness		normal distribution				Chebyshev's theorem			
	mean thickness [mm]	standard deviation [mm]	mean thickness [mm]	error [%]	mean thickness [mm]	error [%]	standard deviation [mm]	Error [%]	mean thickness [mm]	error [%]	standard deviation [mm]	Error [%]
Plate #1	12.894	3.619	11.7	9.26	13.5	4.70	4.5	24.34	12.0	6.93	3.5	3.29
Plate #2	12.294	4.031	13.1	6.55	13.0	5.74	4.1	1.71	12.0	2.39	3.8	5.73
Plate #3	9.7	5.382	24.1	148.45	12.8	31.96	5.5	2.19	11.0	13.4	5.5	2.19
Plate #4	7.106	3.619	5.6	21.19	10.6	49.17	3.0	17.10	9.2	29.47	3.5	3.29

Table 3
Comparison of exact and estimated parameters based on numerical results under different assumptions about thickness distribution.

	exact statistic parameters		assumption of average, constant thickness		normal distribution				Chebyshev's theorem			
	mean thickness [mm]	standard deviation [mm]	mean thickness [mm]	error [%]	mean thickness [mm]	error [%]	standard deviation [mm]	Error [%]	mean thickness [mm]	error [%]	standard deviation [mm]	Error [%]
Plate #1	12.894	3.619	25.2	95.44	9.0	30.20	3.0	17.10	12.6	2.28	3.6	0.53
Plate #2	12.294	4.031	29.5	139.95	10.4	15.41	3.0	25.58	12.6	2.49	3.0	25.58
Plate #3	9.700	5.382	40.0	312.37	12.8	31.96	5.0	7.10	7.8	19.59	3.5	34.97
Plate #4	7.106	3.619	34.5	385.51	10.6	49.17	5.0	38.16	8.4	21.02	3.3	8.81

error was less than 14 %.

5. Discussion and conclusions

This paper investigates the influence of thickness variability on guided wave propagation in plates with non-uniform geometry. The study combines experimental, numerical, and theoretical approaches to evaluate the relationship between plate thickness distributions and wave velocity.

Plates with controlled thickness variations, defined by a sine function, were fabricated and analyzed. The sine-shaped plates used in this study were effective in controlling thickness variability while minimizing unwanted reflections and mode conversions. On the other hand their shape defined in that way provided that their thickness distribution could not be described by normal distribution. Additionally, the thickness variability provided that differences in wave propagation velocity in all plates.

The first stage of the study demonstrated that plate thickness variability has a significant impact on guided wave propagation velocities. Plates with higher mean thickness and lower variability, such as Plates #1 and #2, exhibited smaller errors in both theoretical and experimental predictions. Conversely, Plates #3 and #4, which had lower mean thickness and higher variability, showed greater deviations, emphasizing the importance of accurately modeling thickness distribution. The use of simplified assumptions to predict wave velocity in such complex structures resulted in only approximate outcomes. In most cases, a more accurate approach involved calculating velocity based on exact thickness distributions or, at the very least, using distributions generated according to Chebyshev's theorem, which requires knowledge of only the key statistical parameters—namely, the mean thickness and standard deviation.

The next stage of the study focused on solving the inverse problem, formulated to determine the statistical parameters of the thickness distribution based on wave velocity measurements across a given frequency range. The results were compared with actual values obtained from the thickness histograms of the tested plates. The analysis aimed to identify distribution parameters such that the resulting dispersion curve differed as little as possible from the experimentally obtained curve. Three scenarios were investigated:

(i) approximating the plate as having a uniform thickness,
(ii) assuming a variable thickness that follows a normal distribution, and
(iii) assuming an arbitrary thickness distribution, with the only known information being that it satisfies the conditions of Chebyshev's theorem.

The results clearly indicate that the highest accuracy was achieved when Chebyshev's theorem was applied to generate the thickness distributions. This approach allowed for more precise estimation of both the mean thickness and standard deviation compared to the other methods. In the case of experimental results, the error in mean thickness estimation ranged from 2.39 % to 29.47 %, whereas assuming a constant thickness led to errors ranging from 6.55 % to 148.55 %. Regarding standard deviation estimation, Chebyshev-based distributions achieved agreement within 0.53 % to 35 %, while assuming a constant thickness made it impossible to determine this parameter at all. Using a normal thickness distribution assumption resulted in errors ranging from 4.7 % to 49.17 %.

The numerical results further reinforced the superiority of Chebyshev's theorem, demonstrating even greater advantages in avoiding predefined assumptions about the exact shape of the thickness distribution. This highlights the importance of using generalized statistical approaches when dealing with complex, non-uniform structures.

Although the application of Chebyshev's theorem has yielded promising results, the method does have certain limitations. In practical scenarios, the minimum remaining thickness is a critical parameter for structural integrity, as it directly influences the load-bearing capacity

and overall safety of a component. While the mean thickness and standard deviation provide useful insights into the general pattern of thickness variation, they do not fully account for the presence of localized deep corrosion pits, which can pose a significant risk even if the average thickness appears acceptable.

Existing studies [14,34] emphasize the importance of directly assessing maximum corrosion depth, highlighting the necessity of precisely identifying the minimum thickness rather than relying solely on statistical estimates. To address this issue, the proposed approach could be further refined by incorporating additional analysis techniques specifically aimed at detecting areas of critical thickness reduction. For example, integrating localized ultrasonic measurements or phased array methods alongside the statistical approach could enhance the ability to pinpoint regions with extreme thinning.

Another important challenge arises from the impact of deep pits on wave propagation. Severe thickness reductions can distort wave transmission, leading to additional reflections that complicate signal interpretation. In extreme cases, deep pits may even block wave transmission entirely, preventing reliable measurements between the actuator and the sensor. Consequently, estimating thickness distributions and determining their standard deviations may become significantly more difficult—or even infeasible—in highly corroded structures. Furthermore, it is important to consider how the proposed Chebyshev-based approach performs under more complex wave propagation conditions. In highly corroded or irregularly shaped structures, severe and abrupt thickness reductions can lead to significant mode conversions, wave scattering, and energy loss. These effects are difficult to capture with global statistical parameters alone, as they introduce localized distortions that impact signal quality and complicate velocity estimation. While the current study focused on relatively smooth and controlled thickness variations to establish a foundational understanding, future research should explore how the method behaves in scenarios involving discontinuities, irregular pit geometries, and mixed-mode propagation. Numerical modeling of such conditions, combined with targeted experimental validation, would offer valuable insights into the robustness and limitations of the Chebyshev-based strategy in real-world applications.

Finally, it should be emphasized that even in cases where localized corrosion is severe (e.g., deep pitting), if it affects only a small fraction of the monitored area, its influence on average wave velocity—and thus on the estimated mean thickness and standard deviation—may be negligible. In such cases, the proposed approach could potentially overlook critical damage due to its reliance on global parameters. This highlights an inherent limitation of average-based methods: they may fail to capture localized anomalies that do not significantly impact global propagation characteristics. For this reason, in practical applications where pitting corrosion or other small-scale defects are expected, it is essential to supplement the statistical approach with localized inspection techniques capable of identifying discrete, high-risk areas.

Future work should focus on developing hybrid methodologies that combine statistical modeling with localized, high-resolution diagnostic techniques to ensure a more comprehensive and accurate assessment of structural health.

Ethical Statement

The authors state that the research was conducted according to ethical standards.

CRediT authorship contribution statement

Beata Zima: Writing – original draft, Visualization, Validation, Supervision, Software, Methodology, Investigation, Funding acquisition, Formal analysis, Conceptualization. **Jochen Moll:** Writing – review & editing, Resources.

Declaration of competing interest

The authors declare that they have no known competing financial interests or personal relationships that could have appeared to influence the work reported in this paper.

Acknowledgment

The research was carried out within project No. 2021/43/D/ST8/00786, financed by the National Science Centre, Poland. Abaqus calculations were carried out at the Academic Computer Centre in Gdańsk.

Data availability

Data will be made available on request.

References

[1] Z. Yang, H. Yang, T. Tian, D. Deng, M. Hu, J. Ma, D. Gao, J. Zhang, S. Ma, L. Yang, H. Xu, Z. Wu, A review on guided-ultrasonic-wave-based structural health monitoring: from fundamental theory to machine learning techniques, Ultrasonics 133 (2023) 107014, https://doi.org/10.1016/J.ULTRAS.2023.107014.
[2] S. Yu, K. Luo, C. Fan, K. Fu, X. Wu, Y. Chen, X. Zhang, Advancing spacecraft safety and longevity: a review of guided waves-based structural health monitoring, Reliab Eng Syst Saf 254 (2025) 110586, https://doi.org/10.1016/J.RESS.2024.110586.
[3] F. Ricci, E. Monaco, N.D. Boffa, L. Maio, V. Memmolo, Guided waves for structural health monitoring in composites: a review and implementation strategies, Prog. Aerosp. Sci. 129 (2022), https://doi.org/10.1016/j.paerosci.2021.100790.
[4] M. Jayawardhana, X. Zhu, R. Liyanapathirana, U. Gunawardana, Compressive sensing for efficient health monitoring and effective damage detection of structures, Mech Syst Signal Process 84 (2017), https://doi.org/10.1016/j.ymssp.2016.07.027.
[5] D. Samaratunga, R. Jha, S. Gopalakrishnan, Wavelet spectral finite element for modeling guided wave propagation and damage detection in stiffened composite panels, Struct Health Monit 15 (2016), https://doi.org/10.1177/1475921716640468.
[6] L. Li, P. Fromme, Mode conversion of fundamental guided ultrasonic wave modes at part-thickness crack-like defects, Ultrasonics 142 (2024) 107399, https://doi.org/10.1016/J.ULTRAS.2024.107399.
[7] S. Wang, Z. Tao Luo, J. Jing, Z. Hao Su, X. Kai Wu, Z. Hua Ni, H. Zhang, Real-time determination of elastic constants of composites via ultrasonic guided waves and deep learning, Measurement (lond) 200 (2022), https://doi.org/10.1016/j.measurement.2022.111680.
[8] M. Sale, P. Rizzo, A. Marzani, Semi-analytical formulation for the guided waves-based reconstruction of elastic moduli, Mech Syst Signal Process 25 (2011) 2241–2256, https://doi.org/10.1016/j.ymssp.2011.02.004.
[9] W. Gao, C. Glorieux, J. Thoen, Laser ultrasonic study of Lamb waves: determination of the thickness and velocities of a thin plate, Int J Eng Sci 41 (2003) 219–228, https://doi.org/10.1016/S0020-7225(02)00150-7.
[10] H. Lamb, On the vibrations of an elastic sphere, Proceedings of the London Mathematical Society s1-13 (1881). doi: 10.1112/plms/s1-13.1.189.
[11] L. Pochhammer, Ueber die fortpflanzungsgeschwindigkeiten kleiner schwingungen in einem unbegrenzten isotropen kreiscylinder, J. Reine Angew. Math. 1876 (1876), https://doi.org/10.1515/crll.1876.81.324.
[12] M. Al Nuwairan, The exact solutions of the conformable time fractional version of the generalized Pochhammer–Chree equation, Mathematical Sciences 17 (2023), https://doi.org/10.1007/s40096-022-00471-3.
[13] A. Farhidzadeh, S. Salamone, Reference-free corrosion damage diagnosis in steel strands using guided ultrasonic waves, Ultrasonics 57 (2015) 198–208, https://doi.org/10.1016/J.ULTRAS.2014.11.011.
[14] T. Pialucha, B. Pavlakovic, D. Alleyne, P. Cawley, Quantitative measurement of remnant thickness in corrosion under pipe supports, Insight: Non-Destructive Testing and Condition Monitoring 62 (2020), https://doi.org/10.1784/insi.2020.62.11.642.
[15] B. Zima, J. Moll, Corrosion damage identification based on the symmetry of propagating wavefield measured by a circular array of piezoelectric transducers: theoretical, experimental and numerical studies, Mech Syst Signal Process 217 (2024), https://doi.org/10.1016/j.ymssp.2024.111538.
[16] Z. Li, J. Yu, X. Zhang, L. Elmaimouni, Guided wave propagation in functionally graded fractional viscoelastic plates: a quadrature-free Legendre polynomial method, Mech. Adv. Mater. Struct. 29 (2022) 2284–2297, https://doi.org/10.1080/15376494.2020.1860273.
[17] L. De Marchi, A. Marzani, N. Speciale, E. Viola, Prediction of pulse dispersion in tapered waveguides, NDT and E Int. 43 (2010), https://doi.org/10.1016/j.ndteint.2009.12.004.
[18] B. Zima, Determination of stepped plate thickness distribution using guided waves and compressed sensing approach, Measurement (lond) 196 (2022), https://doi.org/10.1016/j.measurement.2022.111221.
[19] Nurmalia, N. Nakamura, H. Ogi, M. Hirao, K. Nakahata, Mode conversion behavior of SH guided wave in a tapered plate, NDT and E Int. 45 (2012), https://doi.org/10.1016/j.ndteint.2011.10.004.

[20] J. Moll, Damage localization in composite structures with smoothly varying thickness based on the fundamental antisymmetric adiabatic wave mode, Ultrasonics 71 (2016), https://doi.org/10.1016/j.ultras.2016.06.002.
[21] E.C. El-Kettani, F. Luppé, A. Guillet, Guided waves in a plate with linearly varying thickness: experimental and numerical results, Ultrasonics (2004), https://doi.org/10.1016/j.ultras.2004.01.071.
[22] L. Moreau, J.-G. Minonzio, M. Talmant, P. Laugier, Measuring the wavenumber of guided modes in waveguides with linearly varying thickness, J Acoust Soc Am 135 (2014), https://doi.org/10.1121/1.4869691.
[23] B. Zima, J. Moll, Theoretical and experimental analysis of guided wave propagation in plate-like structures with sinusoidal thickness variations, Arch. Civ. Mech. Eng. 23 (2023), https://doi.org/10.1007/s43452-022-00564-9.
[24] B. Zima, J. Moll, Numerical and experimental investigation of guided ultrasonic wave propagation in non-uniform plates with structural phase variations, Ultrasonics 128 (2023), https://doi.org/10.1016/j.ultras.2022.106885.
[25] X. Zhang, S. Shen, Y. Luo, L. Elmaimouni, J. Yu, Dispersion and attenuation characteristics of Lamb waves in multilayered piezoelectric semiconductor plates with imperfect interfaces, Mech. Adv. Mater. Struct. (2025), https://doi.org/10.1080/15376494.2025.2456681.
[26] R. Tian, J. Liu, E. Pan, Y. Wang, SH waves in multilayered piezoelectric semiconductor plates with imperfect interfaces, Eur. J. Mech. A. Solids 81 (2020) 103961, https://doi.org/10.1016/J.EUROMECHSOL.2020.103961.
[27] C. Xu, P. Wei, Z. Li, X. Guo, Shear horizontal wave propagation on a piezoelectric substrate with periodic gradient local resonant metasurfaces, Appl Math Model 137 (2025) 115733, https://doi.org/10.1016/J.APM.2024.115733.
[28] J. Moll, T. Wandowski, P. Malinowski, M. Radzienski, S. Opoka, W. Ostachowicz, Experimental analysis and prediction of antisymmetric wave motion in a tapered anisotropic waveguide, J Acoust Soc Am 138 (2015), https://doi.org/10.1121/1.4922823.
[29] P.B. Nagy, L. Adler, Surface roughness induced attenuation of reflected and transmitted ultrasonic waves, J. Acoust. Soc. Am. 82 (1987), https://doi.org/10.1121/1.395545.
[30] J.A. Ogilvy, Theoretical comparison of ultrasonic signal amplitudes from smooth and rough defects, NDT Int. 19 (1986) 371–385, https://doi.org/10.1016/0308-9126(86)90028-3.
[31] L. Maio, V. Memmolo, N. Christophel, S. Kohl, J. Moll, Electromechanical admittance method to monitor ice accretion on a composite plate, Measurement 220 (2023) 113290, https://doi.org/10.1016/J.MEASUREMENT.2023.113290.
[32] L. Maio, J. Moll, V. Memmolo, J. Simon, Ultrasonic inspection for ice accretion assessment: effects on direct wave propagation in composite media, Mech Syst Signal Process 173 (2022) 109025, https://doi.org/10.1016/J.YMSSP.2022.109025.
[33] K. Neuschwander, J. Moll, V. Memmolo, M. Schmidt, M. Bücker, Simultaneous load and structural monitoring of a carbon fiber rudder stock: experimental results from a quasi-static tensile test, J Intell Mater Syst Struct 30 (2019), https://doi.org/10.1177/1045389X18806392.
[34] N. Suresh, K. Balasubramaniam, Remnant thickness quantification in small thickness structures utilising the cut-off property of A1 Lamb wave mode employing linear array elements, J Appl Phys 131 (2022), https://doi.org/10.1063/5.0085102.